Band-structure and core-hole effects in resonant inelastic soft-x-ray scattering: Experiment and theory

J. A. Carlisle*
Virginia Commonwealth University, Richmond, Virginia 23284

Eric L. Shirley
National Institute of Standards and Technology, Gaithersburg, Maryland 20899

L. J. Terminello
Lawrence Livermore National Laboratory, Livermore, California 94551

J. J. Jia and T. A. Callcott
University of Tennessee, Knoxville, Tennessee 37996

D. L. Ederer
Tulane University, New Orleans, Louisiana 70118

R. C. C. Perera
Center for X-ray Optics, Lawrence Berkeley National Laboratory, Berkeley, California 94720

F. J. Himpsel
University of Wisconsin-Madison, Madison, Wisconsin 53706
(Received 30 March 1998)

Inelastic x-ray scattering has been observed in the hexagonal forms of carbon (graphite) and boron nitride (hBN), both above and below their K edges. For excitation energies *below* the core threshold, inelastic-loss features are observed, which disperse *linearly* with excitation energy (Raman-like behavior). However, *above* the threshold, emission features that move in a *nonlinear* fashion are observed. We show that these two scattering regimes, which have previously been thought of as separate processes, viz., resonant x-ray Raman scattering (below threshold) and resonant inelastic x-ray scattering (above threshold), are described by the same theory for resonant fluorescence. Simulated spectra, with and without excitonic effects, are presented and compared with experiment. We conclude, based on this comparison, that excitonic effects influence these spectra in two ways. Primarily, the total fluorescence yields are enhanced or reduced simply because of changes in the absorption cross sections. Second, excitonic effects on emission features can be pronounced near some excitonic resonances, and these changes are more significant for excitation further above the K edges, which we attribute to the multiplicity of core-excited states being probed. Based on these findings, we conclude that core-hole effects do not necessarily undermine an interpretation of the scattering in terms of a one-electron (noninteracting) picture, and that resonant fluorescence spectroscopy may be successfully used to probe the band structure of solids. [S0163-1829(99)08911-0]

I. INTRODUCTION

Advances in synchrotron light sources have led to much effort devoted towards the understanding and exploitation of resonant x-ray scattering processes in various systems. Examples include the anomalous x-ray diffraction effect, which has been used to study buried interfaces[1] and magnetic systems,[2] and the resonant Raman effect, which also has been used to study magnetic systems.[3] In most of these *hard*-x-ray based resonance techniques, x-rays scatter via virtual core-hole intermediate states (induced by photon absorption) so that final states also contain a core hole. The information gained is generally insensitive to band structure (or the extended bonding structure).

It has recently been demonstrated theoretically[4–6] and experimentally[7–18] that resonant inelastic x-ray scattering (RIXS) in the soft-x-ray energy regime (50 to 1000 eV), with a core-hole intermediate state but a valence-excited final state, can sensitively probe the electronic structure of a wide range of material systems. This has been a particularly active area of research in the past few years and has fundamentally changed the way x-ray scattering is viewed in the soft-x-ray regime. Resonant soft-x-ray fluorescence, the technique used to observe RIXS, has many intrinsic strengths for characterizing robust material systems, including elemental specificity and the ability to probe deeply (to ~1000 Å) into a material.[8,9] When the scattering involves valence-excited final states, certain selection rules have been shown to arise. For instance, in the fullerenes C_{60} and C_{70}, it is possible to sensitively probe the even/odd symmetry of the first few highest occupied molecular orbitals and lowest unoccupied molecular orbitals using RIXS.[10] In chemisorption systems

such as N_2 on Ni(100) (Ref. 11) and Cu(100),[12] it is possible to isolate the adsorbate molecular orbitals from the bulk and to probe the degree of overlap or coupling between them and the bonding structure of the substrate. Work on diatomic species like O_2 has given further insight into the nature of the RIXS process, in particular the role of the intermediate state in the scattering.[13]

In other cases, in which the core-excited state also involves delocalized Bloch orbitals (i.e., orbitals derived from the continuum of states in the conduction bands), *crystal momentum* can be conserved in the RIXS process, just as is energy. This has led to much interest in RIXS as a probe of band structure in systems where such information is generally inaccessible to other techniques, e.g., insulators or polycrystalline samples.[8] Crystal momentum conservation in RIXS has been observed in many systems: diamond,[4] silicon,[14] silicon carbide,[15] hexagonal boron nitride (hBN),[16] cubic boron nitride,[17] gallium nitride,[18] and, most clearly, in graphite.[6] In graphite, a nonlinear dispersion of the emission features is observed, which can only be the result of crystal momentum conservation and the coherent participation of translationally equivalent intermediate states in the scattering. Much study on this resonant process involving valence electrons has yielded information for excitation energies *above* an x-ray edge. Only recently has it been shown in hBN (Ref. 16) that band-structure information may also be obtained for excitation energies *below* the core threshold, e.g., resonant soft-x-ray Raman scattering without a core hole in the final state.

It might seem surprising that, if the stationary intermediate states are delocalized, RIXS can have a significant cross section compared to emission by a normal, two-step fluorescence process. Such a two-step process may be effectively realized if available scattering mechanisms (e.g., phonons) destroy the coherence of translationally equivalent core-hole excited states. Of greater recent interest, possible roles of intermediate states have been the focus of attention.[5,19,20] Simplistically, we find that core-hole excitation can render a system, over the short time scales of relevance, in a state in which the promoted electron is localized near the core hole, regardless of the electron-core-hole attraction. Here, we show that such core-hole effects (i.e., the attraction) do not perturb the scattering to invalidate a one-electron picture when identifying observed emission features and their changes with excitation energy near absorption thresholds. Many spectral features observed for excitation *both above and below threshold* can be modeled by the same scattering physics, based on the quasiparticle band structure of graphite and hBN and the Kramers-Heisenberg relation. On a finer level of detail, incorporation of core-hole effects into the model resolves some but not all of the remaining disagreements between theory and experiment, *viz.* absorption cross sections and total-fluorescence yields are better realized, especially near absorption thresholds. Hence, we contend that the RIXS technique holds great promise for probing the element-specific, local momentum-resolved electronic structure of insulators, buried thin films and heterointerfaces, and other systems that are difficult to probe using other techniques.

The remainder of the paper is organized as follows. In Sec. II our experimental procedure is discussed, as are the theoretical considerations and methodology used to simulate the observed scattering. In Sec. III, most of the resonant fluorescence data obtained from graphite and hBN are presented, and differences in the resonant behavior between these two systems are discussed. Theoretical simulation of the scattering and a closer examination of ranges of excitation energy of particular interest are presented in Sec. IV. Section V summarizes our results and mentions their implications in regards to future experiments.

II. EXPERIMENTAL PROCEDURE AND THEORETICAL MODEL

A. Experiment

The fluorescence experiments were conducted on Beamline 8.0 at the advanced light source at Lawrence Berkeley National Laboratory.[21] The beamline and the fluorescence spectrometer used in this paper are described in detail elsewhere.[22] Emitted radiation was measured with a Rowland circle-type spectrometer utilizing large spherical gratings and a photon-counting area detector. Total instrumental resolution in the *C* 1s emission region was 0.3 eV (full width at half maximum). The bandwidth of the incident photons used was varied between 60 and 150 meV, as described below. The incident flux was monitored by measuring the current from a gold foil located immediately upstream from the spectrometer. The incident photon energy was calibrated to the known graphite π^* and σ^* and hBN π^* absorption features.[23] The spectrometer energy calibration was accomplished by identifying the elastic peak with the incident photon energy. A typical emission spectrum in this paper was acquired in 10 min. The graphite sample used was highly oriented pyrolytic graphite (HOPG), which was freshly cleaved immediately prior to insertion into the spectrometer. The crushed-powder hexagonal boron nitride (hBN) sample was obtained from a commercial source.

B. Theory

1. Physical model

The fluorescence spectra were interpreted and simulated using the Kramers-Heisenberg formula for light scattering. In the transverse gauge, the interaction of radiation with matter is given by the substitution for the electron kinetic-energy operator,

$$\frac{\mathbf{p}^2}{2m} \rightarrow \frac{\mathbf{p}^2}{2m} + \frac{e}{mc}\mathbf{p}\cdot\mathbf{A} + \frac{e^2}{2mc^2}\mathbf{A}\cdot\mathbf{A}. \tag{1}$$

Because of the experimental geometry, illustrated in Fig. 1, the crossed polarizations of incident and detected radiation obviate further consideration of the $\mathbf{A}\cdot\mathbf{A}$ term. Letting $h\nu$ and $h\nu'$ denote incident and emitted photon energies, with ε and ε' being the photons' electric-field polarization vectors, we may write the formula simply as

$$S(h\nu, h\nu') \propto \sum_{f,\varepsilon'} \delta(h\nu' - h\nu + E_f - E_i) \times \left| \sum_m \frac{\langle f|\mathbf{p}\cdot\boldsymbol{\varepsilon}'|m\rangle\langle m|\mathbf{p}\cdot\boldsymbol{\varepsilon}|i\rangle}{E_i + h\nu - (E_m - i\Gamma_m)} \right|^2, \tag{2}$$

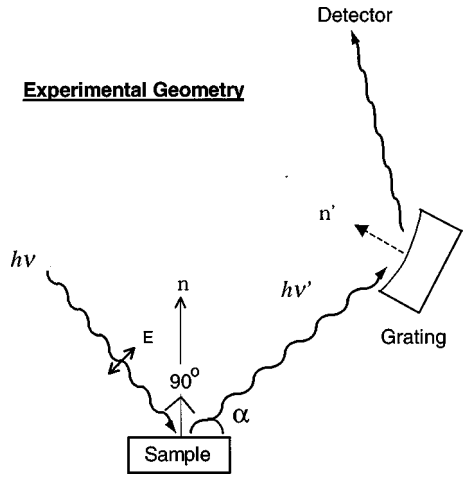

FIG. 1. Schematic of the fluorescence spectrometer used in this paper. The incident-radiation polarization vector lies in the same plane as the grating spectrometer. The take-off angle α is adjusted by rotating the sample as shown.

where $S(h\nu,h\nu')$ is the emission spectrum for a given $h\nu$. The state $|i\rangle$ is the crystalline ground state, m runs over stationary, core-hole-excited intermediate states, and f runs over all stationary final states. Γ_m is a phenomenological inverse-lifetime parameter for state $|m\rangle$ and assumes exponential core-hole decay.

The Stokes shift $h\nu-h\nu'$ is independent of the allowed intermediate channel m by which a final state is reached: it is given by E_f-E_i and *vice versa*. Likewise, conservation of momentum permits identification of a solid's total momentum in the final state. Considerable momentum can be transferred into phonons with minimal accompanying energy transfer. For graphite and other metals, low-energy electronic excitations may also be created during a RIXS experiment. Such considerations can shape one's physical picture of the nature of states $|m\rangle$ and $|f\rangle$, or, conversely, the failure of a given picture to account for observed spectral features can indicate neglect of mechanisms such as phonons.

Our model neglects vibrationally excited intermediate and final states, and considers only certain electronically excited states. States $\{|m\rangle\}$ have a core hole and an electron promoted to the unoccupied bands. States $\{|f\rangle\}$ have a conduction-band electron and a valence-band hole. Electronic multiply excited states, while not considered here, could (in principle) also play a role. Identifying the incident and emitted photon momenta as $\mathbf{q}$ and $\mathbf{q}'$, momentum conservation then dictates the following forms for a state $\{|m\rangle\}$ and a state $\{|f\rangle\}$:

$$|m\rangle=\sum_{S,nk} C_m^{S,n\mathbf{k}} a^+_{n\mathbf{k}+\mathbf{q}} a_{S,\mathbf{k}}|i\rangle\equiv\sum_{S,n\mathbf{k}} C_m^{S,n\mathbf{k}}|S,n\mathbf{k}\rangle, \quad (3)$$

and

$$|f\rangle=\sum_{n,n'\mathbf{k}} D_f^{n,n'\mathbf{k}} a^+_{n\mathbf{k}+\mathbf{q}} a_{n'\mathbf{k}+\mathbf{q}'}|i\rangle, \quad (4)$$

[To clarify the formalism, note that the operator ''$a_{n\mathbf{k}}$'' annihilates an electron in band n at crystal momentum $\mathbf{k}$, and ''$a_{S\mathbf{k}}$'' annihilates a Bloch sum with crystal momentum $\mathbf{k}$ of a core state S in each unit cell. Adjoints of such operators $(a^+_{n\mathbf{k}}, a^+_{S\mathbf{k}})$ correspondingly create particles.]

In an independent-quasiparticle picture, coefficient matrices C and D are assumed to be diagonal. C is not diagonal because of electron-core-hole interactions, i.e., ''core-hole effects.'' D cannot be diagonal because of final-state excitonic effects. We consider core-hole effects in this paper but reserve the more difficult treatment of valence-hole effects to a later paper. This is a satisfactory truncation of electron-hole interaction effects included, because the core-hole effects can be the stronger of the two effects. We will speculate in at least once instance, however, about a possible signature of final-state electron-hole interactions, because these influence final-state cross sections.

2. Algorithmic implementation

To formulate constituents of the above Kramers-Heisenberg picture more concretely, we model (1) core states, (2) band states, (3) the $\mathbf{p}\cdot\mathbf{A}$ matrix elements, and (4) core-hole effects as follows:

(1) Core states are simple in these systems, being the C 1s, B 1s, and N 1s levels. Suitable one-electron orbitals are found in atomic Hartree-Fock calculations. These orbitals may be used to determine $\mathbf{p}\cdot\mathbf{A}$ matrix elements and core-hole effects.

(2) The band states are constructed within a pseudopotential/plane-wave local-density approximation (LDA) framework, but with two qualifications, as described below. The particular type of pseudopotential/plane-wave calculation is described in Ref. 24. We used 100 ''optimal'' basis functions, which were optimized to describe the Bloch functions of eight valence and twelve conduction bands.

The first qualification involves the band energies used. Because LDA band energies have intrinsic inaccuracies, appropriate self-energy corrections are added to improve band energies. Corrections for graphite are taken from Zhu and Louie,[25] and, for hBN, from Blase *et al.*[26] In graphite, the corrections are mostly a $\pm 14.5\%$ enhancement of the energy difference between a given band energy and the Fermi energy E_F. However, applying this rule places these σ^* band minimum at M about 1 eV too high compared to Zhu and Louie's result. For hBN, the band gap is increased by 1.5 eV because of self-energy effects, and the valence bandwidth is enhanced by $\sim 14.6\%$.

The second qualification involves the evaluation of electron properties within the atomic-core region. To evaluate properties that are dependent on a precise orbital, a pseudopotential inversion scheme was developed. The behavior of the wave function was assumed to be that of a combination of low l partial waves described by valence $2s$, $2p$, $3s$, and $3p$ orbitals' radial dependencies. Suppose that a given Bloch function $\psi_{n\mathbf{k}}$ has the following behavior for small $|\mathbf{r}|$:

$$\psi_{nk}(\mathbf{r})=\sum_\nu E_\nu^{n\mathbf{k}}\Phi_\nu(\mathbf{r})=\sum_\nu E_\nu^{n\mathbf{k}} Y_\nu(\hat{\mathbf{r}})\varphi_\nu(|\mathbf{r}|). \quad (5)$$

Here, ν runs over valence states, and the atomic nucleus is assumed to be at the origin, and atomic orbitals or their angular and radial dependencies are implied. In the pseudopotential band calculation, we should have an analogous

$$\psi^{PP}_{n\mathbf{k}}(\mathbf{r})=\sum_\nu F_\nu^{n\mathbf{k}} Y_\nu(\hat{\mathbf{r}})\varphi^{PP}_\nu(|\mathbf{r}|). \quad (6)$$

The identification, $E_\nu^{n\mathbf{k}}=F_\nu^{n\mathbf{k}}$, permits the determination of the true electron orbitals when computing $\mathbf{p}\cdot\mathbf{A}$ matrix elements and electron-core-hole interaction effects. Coefficients $\{E_\nu^{n\mathbf{k}}\}$ can be found by analyzing a Bloch function and true- and pseudoatomic orbitals.

(3) While detailed evaluation of the $E_\nu^{n\mathbf{k}}$'s may be carried out, the $\mathbf{p}\cdot\mathbf{A}$ matrix elements may also be deduced with sufficient accuracy (aside from a proportionality constant) from the gradient of a band state at the nucleus of a given site. This gradient approach was used throughout this paper, and subsequent tests that involved the above, more detailed analysis of the Bloch function justified the approach. More accurately, one has

$$\langle m|\mathbf{p}\cdot\mathbf{A}|i\rangle=\sum_{S,n\mathbf{k}}(C_m^{S,n\mathbf{k}})^*\sum_\nu(E_{S\nu}^{n\mathbf{k}+\mathbf{q}})^*\langle\Phi_\nu|\mathbf{p}\cdot\mathbf{A}|1\mathrm{s}\rangle, \quad (7)$$

and

$$\langle f|\mathbf{p}\cdot\mathbf{A}|m\rangle=\sum_{S,nk}C_m^{S,n\mathbf{k}}\sum_{n',\nu}D_f^{nn'\mathbf{k}}E_{S\nu}^{n'\mathbf{k}+\mathbf{q}'}\langle 1s|\mathbf{p}\cdot\mathbf{A}|\Phi_\nu\rangle, \quad (8)$$

where the E coefficients are now also specified by atomic site (implied by S). The above formulas relate $\mathbf{p}\cdot\mathbf{A}$ matrix elements found in the Kramers-Heisenberg expression to atomic transition dipoles.

(4) Noting that the two-particle (electron-core-hole) interaction matrix is block diagonalized with respect to core site, the matrix element can be computed by assuming that the core hole is localized on one site in the crystal. This localization may only be used to compute an interaction matrix element, whereas a $\mathbf{p}\cdot\mathbf{A}$ operator forces one to consider a coherent sum of corresponding intermediate states in the Kramers-Heisenberg expression. While x-ray absorption spectroscopy (XAS) is sensitive only to the relative electron-core-hole localization, a full description of RIXS in a crystalline solid involves both such localization and a definition of the solid's total crystal momentum, because interference between x-rays emitted at different atomic sites can occur.

Except for the core-hole effects, everything mentioned in Eqs. (1)–(3) is considered in an independent-quasiparticle picture of RIXS. Core-hole effects can be incorporated through the replacement,

$$H_0\rightarrow H=H_0+V_D+V_X, \quad (9)$$

where H_0 is the independent-quasiparticle Hamiltonian for intermediate, core-hole-excited states. Obviously, we have

$$\langle S',n'\mathbf{k}'|H_0|S,n\mathbf{k}\rangle=\delta_{S,S'}\delta_{n,n'}\delta_{\mathbf{k},\mathbf{k}'}(\varepsilon_{nk}-\varepsilon_S), \quad (10)$$

where $\varepsilon_{n\mathbf{k}}$ is a band energy, and ε_S is a core-level energy.

By V_D and V_X, we denote the direct and exchange parts of the electron-core-hole interaction. The screened, electrostatic attraction is included in V_D. V_X results from the absence of an attractive exchange interaction between a core electron and band state, because of the core-level vacancy. We may find matrix elements of V_X readily, because they are given by

$$\langle S,n\mathbf{k}|V_X|S',n'\mathbf{k}'\rangle=2\,\delta_{S,S'}\sum_{\nu,\nu'}(E_{S,\nu}^{n\mathbf{k}+\mathbf{q}})^*(E_{S,\nu}^{n'\mathbf{k}+\mathbf{q}'})\times\langle 1\mathrm{s},\nu|V|\nu',1\mathrm{s}\rangle, \quad (11)$$

where the right-most matrix element is a standard atomic-exchange integral.

Matrix elements of V_D could be found by rewriting them as

$$\langle S,n\mathbf{k}+\mathbf{q}|V_D|S',n'\mathbf{k}'+\mathbf{q}'\rangle=\delta_{S,S'}\langle\psi_{n\mathbf{k}+\mathbf{q}}|V_D(S)|\psi_{n'\mathbf{k}'+\mathbf{q}'}\rangle, \quad (12)$$

which involves a matrix element between two Bloch states of the screened potential of a $a+e$ charge located on the site specified by S. In Ref. 5, the screened potential was computed using the Levine-Louie-Hybertsen model for dielectric screening.[27] In many cases, this model describes both the correct short- and long-range behavior of a screened potential and realistically accounts for the different screening response of atoms, bonds, and interstitial regions in real crystals. However, a more complete accounting for the screened potential has indicated that better results were obtained by using an atomically screened core-hole potential. Such a potential was computed from the change in the total charge density of a free atom or ion upon removal of a 1s electron. This potential was supplemented by that of a shell of charge $-e(1-1/\varepsilon_\infty)$, where ε_∞ is the static dielectric constant (infinite in graphite). The average radius of such a shell was adjusted empirically so that measured and computed absorption spectra were similar. In this way, inclusion of the correct degree of core-hole effects was assured with minimal empiricism. While $V_D(\mathbf{r})$ depends both on the distance and direction of a point $\mathbf{r}$ from a core-hole's site, the directional dependence may be neglected without major approximation. By fitting $V_D(\mathbf{r})$ with a form amenable to analytical Fourier transformation, the complete Fourier decomposition of Bloch states and V_D permits straightforward evaluation of all desired matrix elements of V_D.

The sizes of secular equations to be solved when inverting $E+h\nu-H$ necessitate use of iterative methods to find the coherent superpositions of $|m\rangle$'s that would be created in an RIXS experiment. Obviously, these superpositions are independent of a final state $|f\rangle$ considered, and $S(h\nu,h\nu')$ is found by carrying out the required summation over f and ε' following evaluation of such superpositions. Further details of numerical aspects of this paper are found elsewhere.[5] It is also helpful, when analyzing core-hole effects on RIXS, to study such effects on XAS. To this end, finding the appropriate $\mathbf{p}\cdot\mathbf{A}$-weighted partial density of states of H by iterative methods has been used.

3. Kinematical considerations

Considerations involving the conservation of momentum and energy and densities of states can facilitate an intuitive understanding of RIXS in a crystalline solid. We have already noted that, barring dissipative effects such as phonons, $\mathbf{q}-\mathbf{q}'$ determines the net total electronic momentum of the final state. For first-row K edges, momenta $\mathbf{q}$ and $\mathbf{q}'$ are small compared to Brillouin-zone dimensions, so that the intermediate and final states are created by nearly vertical transitions. This simplicity helps facilitate investigation of the band structure of a material using RIXS. In particular, it

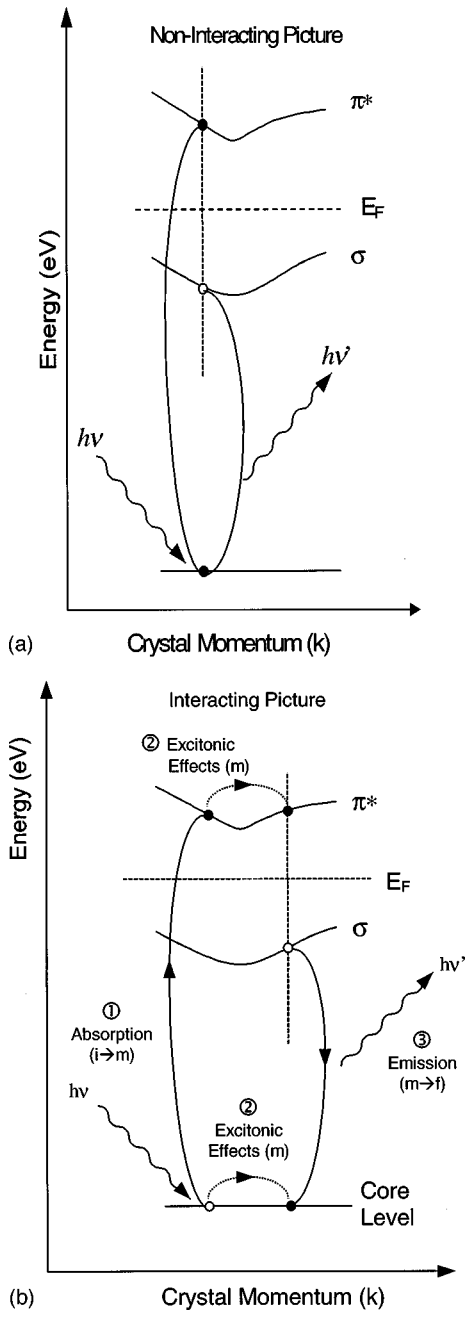

FIG. 2. Schematic of the RIXS process in a noninteracting picture [Fig. 2(a)] and in an interacting picture [Fig. 2(b)]. This figure shows schematically the intermediate states by which the inelastic resonance x-ray scattering process occurs. These are core-excited states, which involve virtual transitions of a core electron to unoccupied conduction band states, as well as core-hole exciton states, which can be either band resonances or be energetically separated from the conduction band. The observed emission features correspond to recombinations of valence electrons with nearly the same crystal momentum as the core hole. The final state of the system has no core hole but a valence hole-conduction electron pair (possibly a valence exciton).

is the combination of the momentum selectivity of RIXS and its intrinsic energy selectivity, which follows from the Kramers-Heisenberg formula, that enables RIXS to be a band-probing tool.

To aid the discussion, Fig. 2 gives energy-level diagrams depicting the RIXS process, as viewed from a picture that does not include core-hole effects [Fig. 2(a)], and as viewed when such excitonic effects are taken into account [Fig. 2(b)]. In the noninteracting picture, the incident photon promotes the core electron, perhaps virtually, to a conduction band, so that the core hole and electron can each have a well-defined crystal momentum. In Fig. 2(b), the electron-core-hole attraction causes the particles to scatter off each other, so that the particles can ''move together'' throughout the Brillouin zone, but their combined, total crystal momentum is still conserved.

Let us temporarily set aside the core-hole effects. Then, for excitation below the core threshold, the RIXS process involves a relatively uniform sum over many intermediate states. However, for excitation above threshold, transitions from the core level to the conduction band that nearly conserve energy are resonantly enhanced by the energy denominator in the Kramers-Heisenberg expression, over a range of energies with a width comparable to the core-hole width. In either case, the system can then relax via a radiative transition of a valence electron to fill the core level. Thus, it is because of the finite dispersion of the low-lying conduction bands that non-Raman-like, nonlinear dispersive behavior is observed for excitation energies above threshold.[6]

Continuing to reason within a noninteracting picture, the above arguments may be quantified if appropriate wave functions are substituted into the Kramers-Heisenberg formula. Energy conservation requires that the energies of the incident and emitted photons be related to the energies of the final-state electron and valence hole by

$$h\nu' - h\nu \cong \varepsilon_{n'\mathbf{k}'} - \varepsilon_{n\mathbf{k}}, \tag{13}$$

where the equality is approximate because of effects neglected. Momentum conservation relates $\mathbf{q}$ and $\mathbf{q}'$ to the *crystal momentum* of the electron and hole, where $\mathbf{G}$ is a reciprocal-lattice vector:[4]

$$\mathbf{q} - \mathbf{q}' = \mathbf{k} - \mathbf{k}' + \mathbf{G}. \tag{14}$$

For $h\nu$ below an x-ray edge, there is no emission resembling ordinary fluorescence, because all intermediate states are virtual. Energy conservation implies that inelastic scattering features track with (i.e., move linearly with) the excitation energy $h\nu$, and the energy loss is the *energy difference* between band states at nearly equal crystal momenta. This situation is analogous to optical Raman spectroscopy, wherein a partial phonon density of states (DOS) tracks linearly with the elastically scattered laser light. Observed intensities are modified by the matrix elements and the energy denominator in Eq. (1), so that the profile of the emission is a partial joint density of states (p-JDOS).

For excitation above an x-ray edge, the energy denominator, which possesses no minima below the core threshold, now resonantly enhances intermediate states, which have energies $E_m \equiv h\nu + E_i$, so that intermediate states for which one has

$$h\nu \cong \varepsilon_{n\mathbf{k}} - \varepsilon_S, \tag{15}$$

over a energy range comparable to Γ_m, will be predominant in the absorption-emission process. The effective energy range will also be affected by the range of experimentally

accepted $h\nu$. Such resonance-induced energy selection leads to electron-state crystal momentum *selectivity*, in addition to conservation of total momentum for excitation above threshold. When this selection occurs, the predominant emission can be at energies given by the deduced relation,

$$h\nu' \cong \varepsilon_{n'\mathbf{k}'} - \varepsilon_S . \tag{16}$$

Again one has $\mathbf{k} \cong \mathbf{k}'$, but the favored values of crystal momentum do not span the entire zone, and are clustered near conduction band isoenergy contours. Crystal momentum-resolved information may be inferred from observed, nonlinear dispersion of emission features, which follows from the band structure.

Now consider Fig. 2(b) which shows the RIXS process in the interacting picture. Here, the available intermediate states belong to a more realistic set, which takes into account the effect of the core hole on the electronic structure near a core-excited atom. The core hole and electron do not individually have unique crystal momenta. If the stationary core-hole-excited states are band resonances, then their wave functions are delocalized in the sense that they have a finite amplitude for arbitrarily large electron-core-hole separation. Bound core-hole excitons can also play a role as intermediate states. Furthermore, through electron-hole localization, it is conceivable, with regard to the matrix elements appearing in the Kramers-Heisenberg formula, for bound states or localized superpositions of resonances to dominate the scattering.

Core-hole effects may play the role of either a weak or on a strong perturbation to the noninteracting Hamiltonian. The relevant criterion for their strength depends on the quantity in which one is interested. It is well established that to describe XAS core-hole effects are critical. To describe RIXS total fluorescence yields, core-hole effects are likewise critical, which is reasonable, because resonant fluorescence must be preceded by the initial excitation probed by XAS. Indeed, core-hole effects enhance simulated XAS cross sections and corresponding total fluorescence yields nearly equally. However, XAS involves a sum over core-hole excited states, which is carried after squaring first-order $\mathbf{p}\cdot\mathbf{A}$ matrix elements, whereas RIXS involves a different sum, which is squared following summation of second-order terms. RIXS emission features are not so much affected by stationary intermediate states as by the coherent superposition of such states, which appear in the Kramers-Heisenberg formula. We may refer to such a superposition as a single ''intermediate state'' of the system, although this state is not a stationary state. Such a superposition can be less affected, aside from its normalization, than are individual, stationary core-hole-excited states. Because of this, a sensible interpretation of RIXS emission features might start from a noninteracting picture. In particular, we note that the interacting and noninteracting intermediate stationary states span the same space of core-hole excited states, and differ only by being the respective solutions of H and H_0.

Stationary states found in an interacting picture will be composed mostly of noninteracting states, that lie within some energy range specified by the interactions' strength. Far from resonance, such intermediate states will be weighted in essentially the same fashion in the Kramers-Heisenberg formula independent of interaction effects. Even on resonance, the superposition of stationary interacting states and of stationary noninteracting states can bear great similarity to each other, and we find that they often do.

Such similarity is motivated by the following observation. The superposition of noninteracting intermediate states that can be coupled radiatively to the final states can be written as

$$|A(h\nu)\rangle \approx \frac{1}{E_i + h\nu - H_0 + i\eta}\mathbf{p}\cdot\mathbf{A}|i\rangle, \tag{17}$$

where we have inverted the matrix $E_i + h\nu - H_0 + i\eta$, and η is a typical inverse-lifetime parameter for the core-hole excited states. The analogous superposition of interacting states is given by

$$|B(h\nu)\rangle \approx \frac{1}{E_i + h\nu - H_0 + i\eta}\left[1 + (V_D + V_X) \times \frac{1}{E_i + h\nu - H + i\eta}\right]\mathbf{p}\cdot\mathbf{A}|i\rangle. \tag{18}$$

$|A(h\nu)\rangle$ and $|B(h\nu)\rangle$ would be proportionate, and hence lead to similar emission spectra, if the actions of $(V_D + V_X)$ and $\mathbf{p}\cdot\mathbf{A}$ leave an electron core-hole pair in similar states. Already, we know that $\mathbf{p}\cdot\mathbf{A}$ must create a pair state in which the core hole and electron are mutually localized, with the electron taking the form of a *p*-like wave packet centered near the core site. Likewise, the electron core-hole interaction is large predominantly at very close range, so it projects out a state with the electron concentrated near the core hole. Then, the left-most operator can select the unoccupied band states, which are the most closely resonant at a given $h\nu$. If this energy selection filters states belonging to only one partial-wave channel (e.g., $l=1$ and $m=0$), $|A(h\nu)\rangle$ and $|B(h\nu)\rangle$ will inevitably be nearly proportional. Indeed, such proportionality is exact for an electron-hole pair in a two-band lattice model featuring an on-site electron-hole interaction.

We have observed such proportionality when simulating RIXS with or without core-hole effects in HOPG and hBN, presumably because of the lowest-energy excitations being confined to π^* core-hole excitons or excitonic resonances. This proportionality has broken down for $h\nu$ tuned to the HOPG σ^* resonance and in diamond and cubic BN, presumably because of the many degenerate or nearly degenerate conduction bands and band valleys. For comparison, at least one other paper has found a signature of nonproportionality between $|A(h\nu)\rangle$ and $|B(h\nu)\rangle$ even near the K edge in graphite.[20]

III. EXPERIMENTAL RESULTS

Resonant fluorescence spectra obtained from a highly oriented pyrolytic graphite sample are shown in Fig. 3. The stack plot of the emission spectra show the C K emission region as the incident photon energy ($h\nu$) is varied below and above the C K edge, which is assumed to be at $h\nu = 284.5$ eV.[23] The photon energies are given to the left of each spectrum. The intensities of each emission spectrum have been normalized to the incident photon flux, so that absolute intensity comparisons between spectra may be made in Fig. 3. Note that the energy separation between successive spectra in the stack plots is nonuniform. The choice of emis-

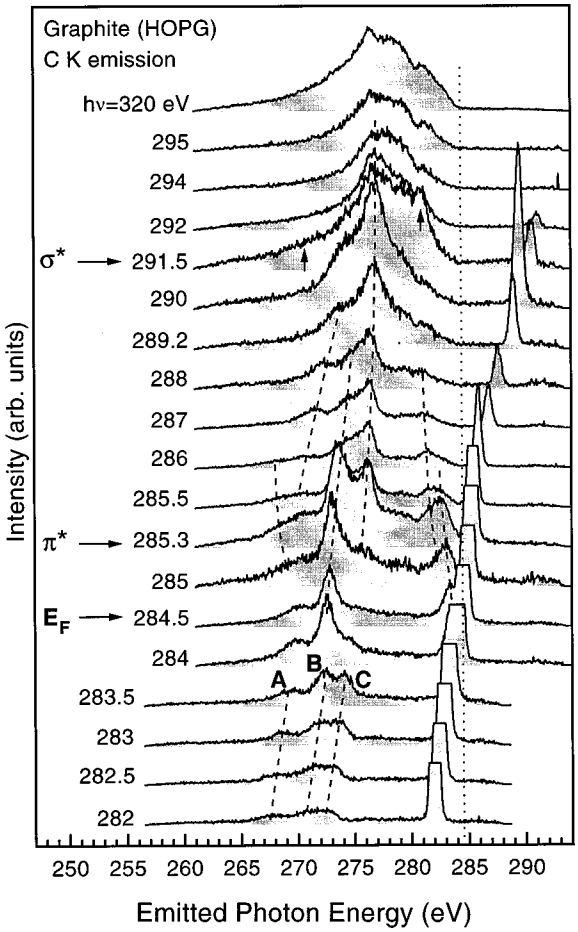

FIG. 3. Resonant fluorescence data obtained from HOPG for incident excitation energies $h\nu$ varied from 281 to 320 eV. The excitation energies are given to the left of each emission spectrum. Note that the spacing between the excitation energies is nonuniform. The width of the incident radiation was approximately $\Delta h\nu = 150$ meV. The dashed lines mark the location of the RIXS peaks.

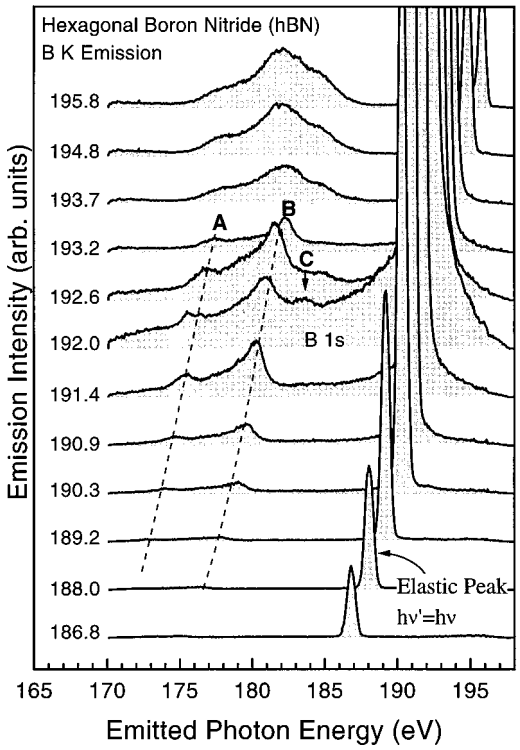

FIG. 4. Resonant fluorescence data obtained from hBN. The excitation energies are given to the left of each spectrum. Note that the spacing between the excitation energies is nonuniform. Features *A*, *B*, and *C* are discussed in the text.

sion geometry ($\alpha = 35°$) allows emission from π bands as well as σ bands.[6]

The emission spectrum obtained for $h\nu = 320$ eV is sufficiently far from the C K edge, so it represents the normal or nonresonant C K emission spectra for graphite. Radiative recombinations with the core hole obey the normal dipole-selection rules, so that this spectrum represents the p ($l = 1$) partial density of states. As expected for the nonresonant fluorescence process, spectral features in this valence emission spectrum correspond to regions with a large density of states in the graphite band structure. The causal connection between incident and emitted x-rays demands that even fluorescence at $h\nu = 320$ eV is described by the Kramers-Heisenberg formula, but our insight into appropriate intermediate states is limited. However, the experimental results suggest that, upon excitation of a core electron far above the K edge, the system is effectively left in a state with no discernible core-hole crystal-momentum selectivity.

In contrast, the resonant emission spectra, obtained when the incident photon energies are near and above the C K edge, exhibit many interesting spectral features, which change in a systematic way with excitation energy. The two regimes for scattering *below* and *above* the core threshold are qualitatively quite different, and can be characterized by the types of dispersive features present. Below threshold, the spectra consist of features that move *linearly* with the excitation energy. These ''loss'' features (borrowing the nomenclature of optical Raman spectroscopy), which occur at a constant energy displacement from the elastic peaks, are labeled *A*, *B*, and *C*, and their displacements from the elastic peak are approximately 16, 12, and 10 eV, respectively.

As the excitation energy moves above the K edge, the nature of the emission changes dramatically. Instead of linear dispersion, the peaks move in a nonlinear fashion. These features are highlighted by the dashed lines in Fig. 3. In fact, some of the features move in a manner opposite to the (increasing) excitation energy. The movement of these features can be directly related to the band structure.[6] Of particular interest in this paper is the behavior of emission spectra as the excitation is tuned so that a core electron is favorably excited near the M and Γ points in the Brillouin zone. This point will be discussed in detail below, in regard to emission by σ and π electrons.

Another interesting feature to note in these valence emission spectra is the intensity behavior of the quasielastic peak. This peak, which ostensibly arises from a direct recombination of the photoelectron with the core hole (leaving the system in the electronic ground state), displays a drastic intensity variation as the excitation energy moves through the core binding energy. This feature will not be discussed further here.

It is interesting now to compare the RIXS in graphite with its structural analog, hBN. Whereas graphite is a semimetal, with an intrinsically *delocalized* electronic structure, hBN is

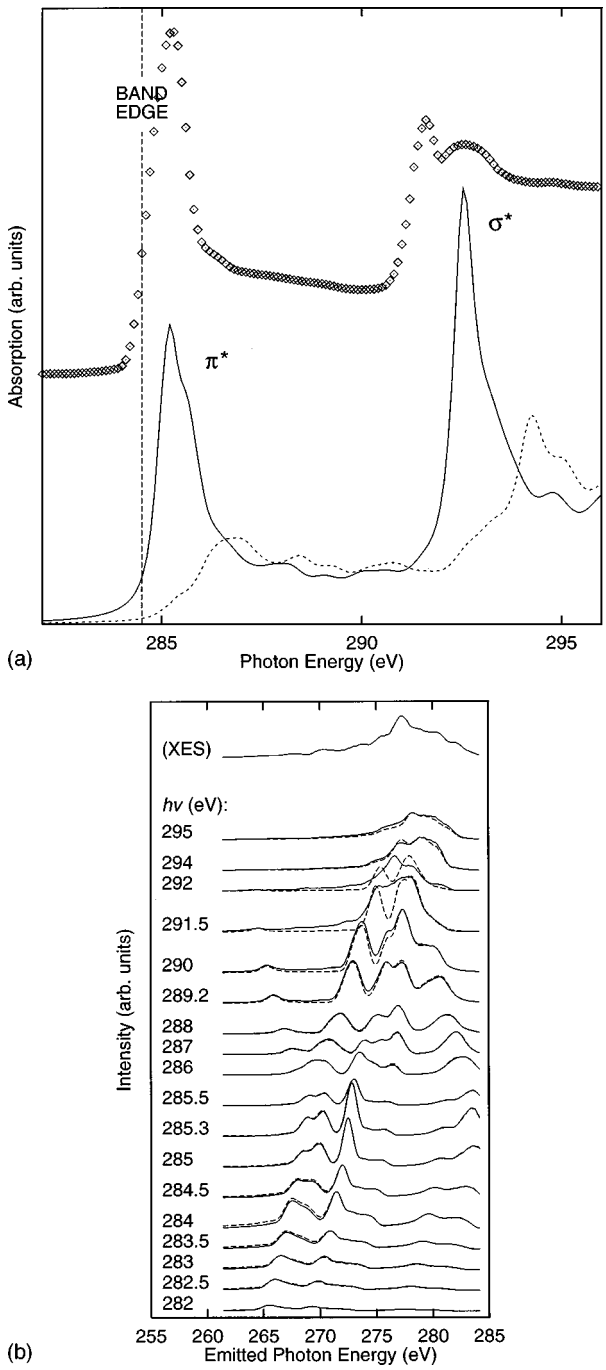

FIG. 5. Simulated x-ray absorption spectrum [Fig. 5(a)] and RIXS [Fig. 5(b)] for graphite. Solid lines correspond to calculations made with core-hole effects included, whereas dashed lines give the results of calculations based on a noninteracting (one-electron) picture. Note that the dashed and solid line are completely overlapped in the RIXS simulation except for excitation energies near the σ^* absorption threshold. XES denotes ordinary fluorescence, which mimics the $h\upsilon = 320$ eV spectrum of Fig. 3.

a wide band-gap semiconductor ($E_g \sim 5.5$ eV); a III-V material wherein the bonding interaction involves significant charge transfer from boron to nitrogen. The empty states in the lowest-lying conduction bands are physically localized near the boron atoms. It is natural then to expect the RIXS to be fundamentally changed owing to the participation of localized intermediate and final states in the scattering. This

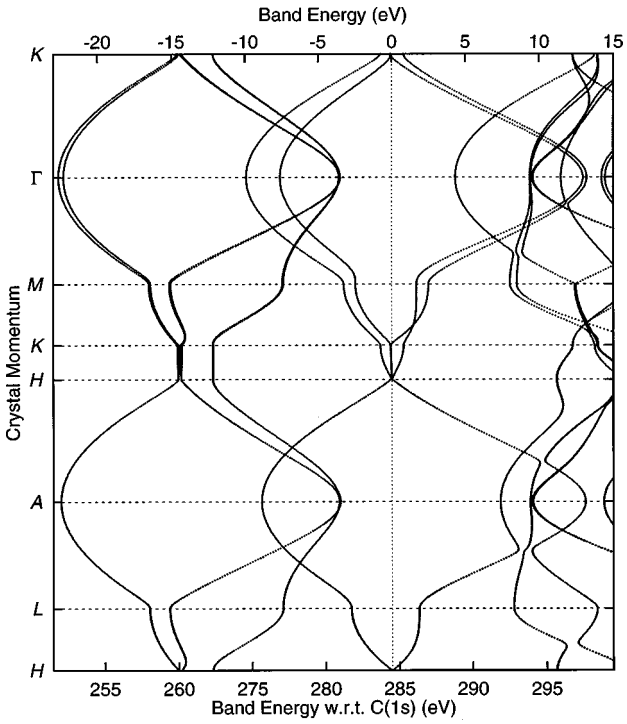

FIG. 6. Band structure of graphite, transposed to facilitate comparison to the experimental and simulated RIXS. The band energies are plotted horizontally with crystal momentum on the vertical axis.

compound also has a well-known strongly bound π^* core-hole exciton, with a binding energy of ~ 1.1 eV.[23]

Figure 4 shows the B K resonant emission spectra from a crushed powder hexagonal boron nitride hBN sample. Again, all spectra have been normalized to the incident photon flux, and labeled by the excitation energy. The elastic peak exhibits a very strong intensity enhancement for $h\nu = 192$ eV, when B 1s electrons are excited into the exciton state involving the B π^* orbital. This feature is detected whenever boron is π bonded in a material, and has been utilized to probe the bonding structure of BN monolayers deeply buried in a C/BN/C multilayer.[28]

Below the core threshold (192 eV), the spectra show two inelastic peaks, labeled *A* and *B*, separated by 5 eV, along with the elastic peak. As was the case in graphite above, these features exactly track the excitation energy, so that the higher energy feature *B* maintains a constant energy separation of about 11 eV from the elastic peak. At threshold, a new feature appears in the spectrum, labeled *C*, about 2.5 eV above peak *B*. At higher incident photon energies, peak *C* is again absent. In sharp contrast to graphite, for excitation above the core threshold ($h\nu \geqslant 193.7$ eV), the emission features abruptly become broadened and fixed in energy position, resembling ordinary B 1s fluorescence for hBN.

In Fig. 4, note also the continuation of the Raman peaks for excitation energies immediately above the B 1s threshold (i.e., the data from $h\nu = 192.0$ to 193.7 eV). Whereas in graphite we have both Raman and non-Raman features for excitation energies corresponding to the core threshold, in hBN the Raman features are the only dispersive ones observed.

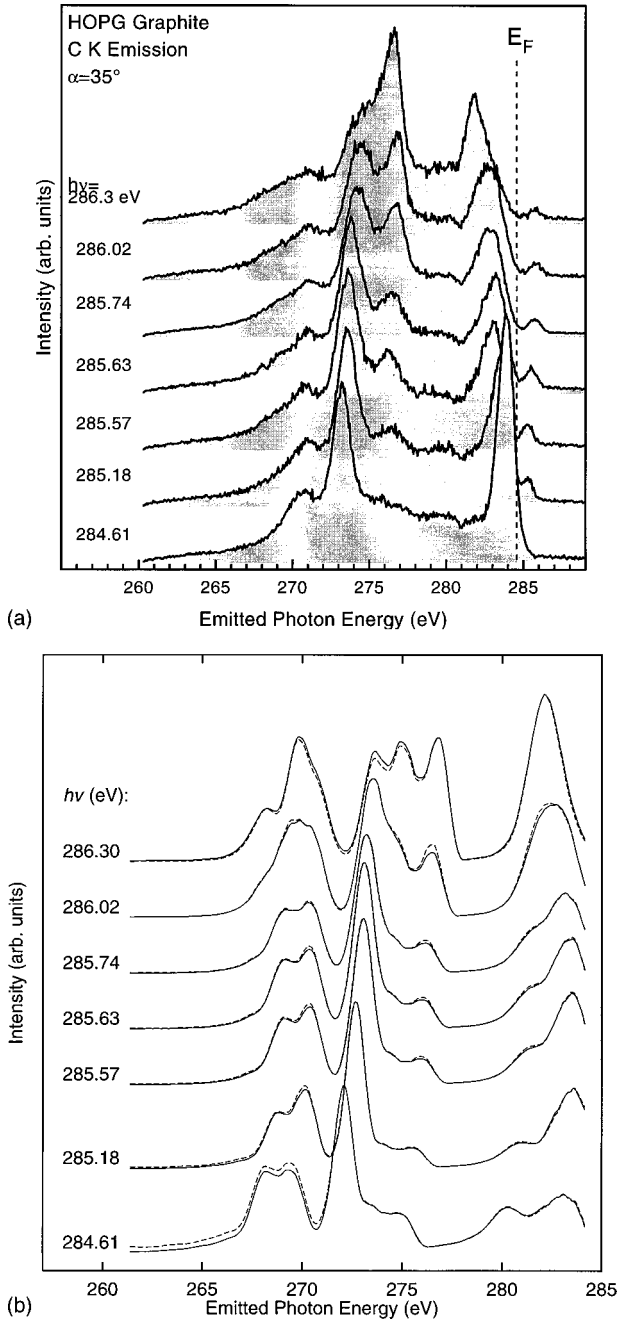

FIG. 7. (a) Experimental RIXS spectra for HOPG collected for excitation energies near the π^* absorption threshold of 284.5 eV. The excitation energies are given to the left of each emission spectrum. The width of the incident radiation has been reduced to $\Delta h\upsilon = 60$ meV. Note the abrupt onset of emission at $h\upsilon = 276$ eV. (b) Theoretical simulations of the data in (a).

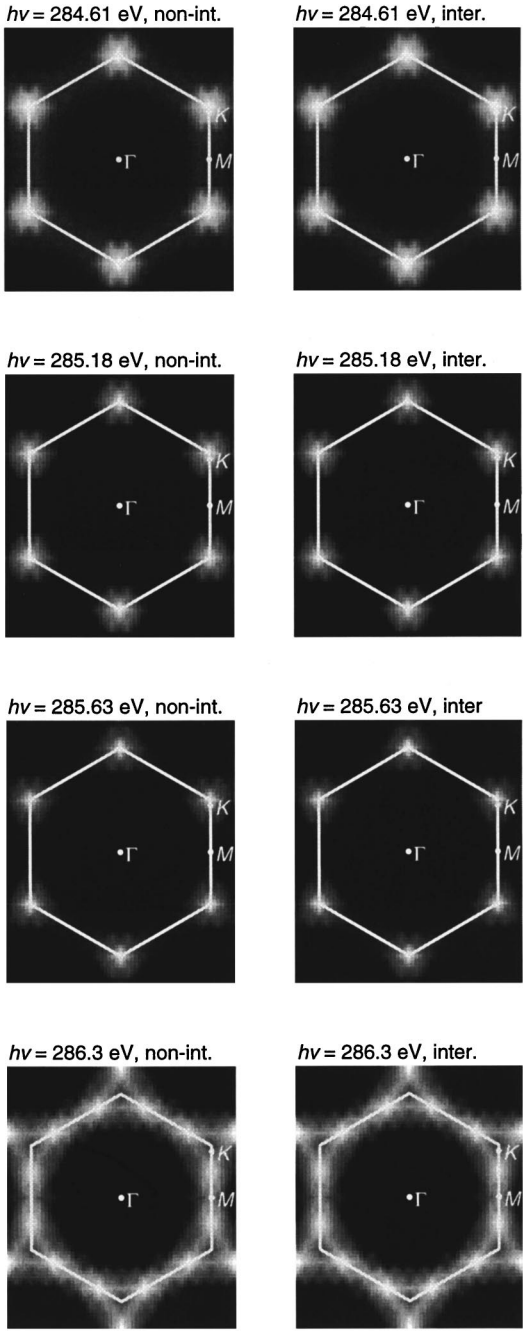

FIG. 8. Simulated crystal-momentum distribution for the core hole in intermediate states in graphite as a function of $h\upsilon$. The excitation energies are those from Fig. 7.

IV. MODELING AND ANALYSIS OF RESONANCES

Simulated XAS and RIXS results for graphite are shown in Fig. 5, and an ''x-y'' transposed band structure is shown in Fig. 6. These theoretical results are presented for 576 sampling points **k** in the first Brillouin zone, and 12 conduction bands were considered for excited electron occupation in intermediate and final states. Results are plotted with solid lines for calculations with core-hole effects included, and with dashed lines for calculations omitting core-hole effects. Our XAS results are similar to those of others.[29] We find an asymmetric σ^* peak in the XAS simulation, but cannot resolve whether the σ^* resonance lies above or below the σ^* threshold. In any event, it is very close to the threshold.

Below $h\nu = 284.5$ eV, which is the assumed K edge, the RIXS spectra exhibit the same Raman-like behavior that is found in experiment. The nominal loss features are found to have 16.3, 12.5, and 9.7 eV Stokes shifts. (The feature with a 4.5 eV Stokes shift is absent when we do not artificially suppress certain interference effects on emission resulting from C $1s \rightarrow \pi$ recombinations. This suppression is discussed further, below.) Above $h\nu = 284.5$ eV, we observe a similar evolution of σ emission as in experiment, with the relative

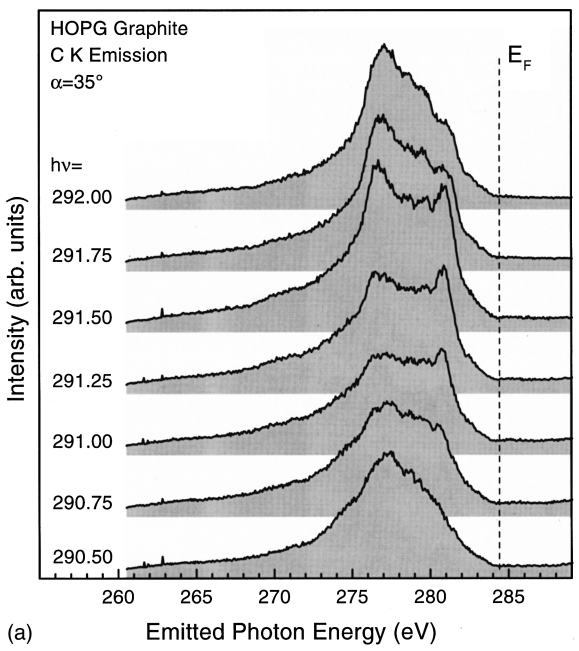

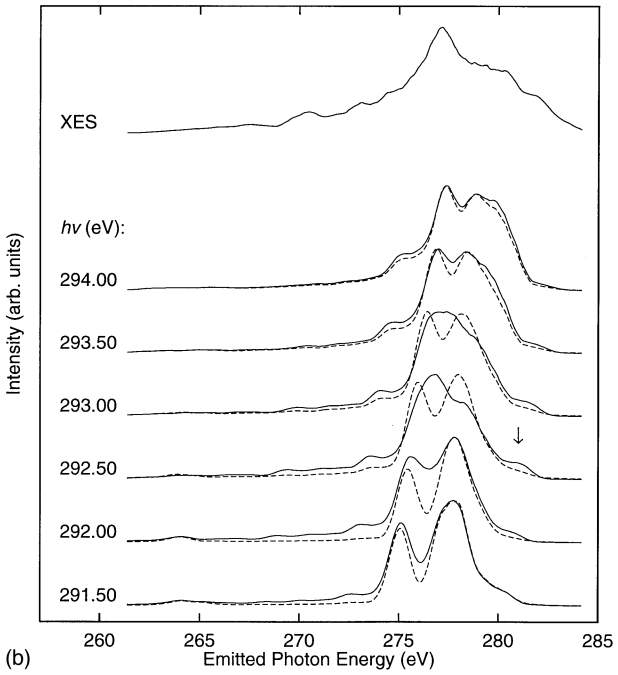

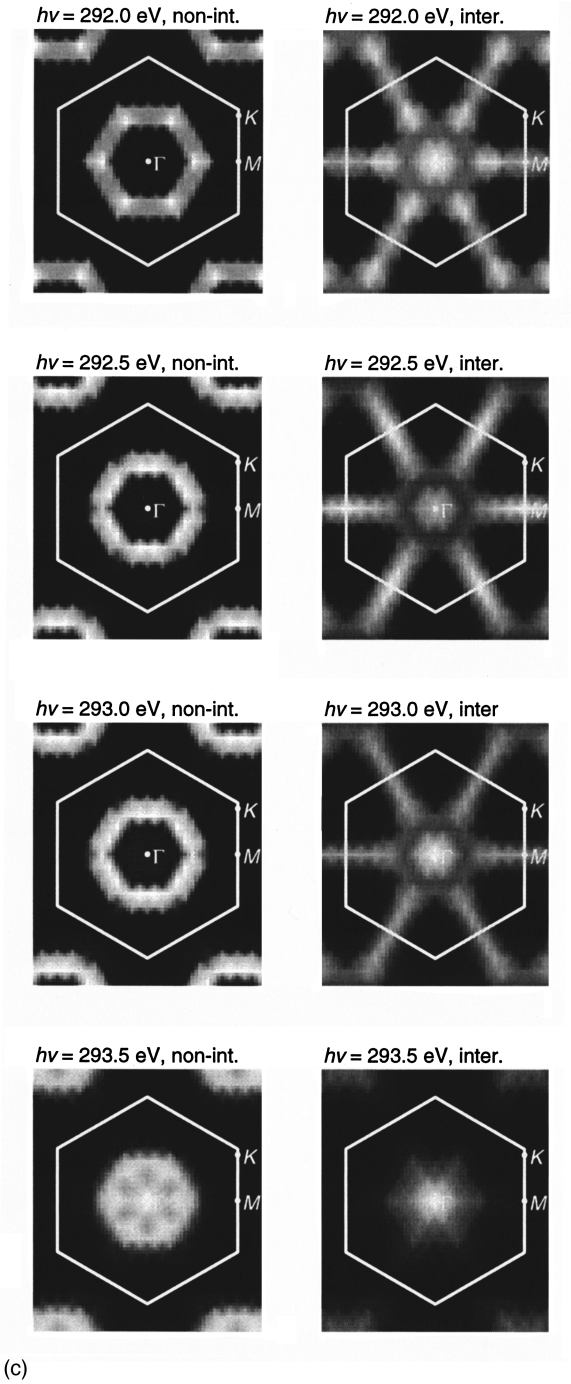

FIG. 9. (a) Experimental RIXS spectra for HOPG collected for excitation energies near the σ^* absorption threshold of 291.6 eV. The excitation energies are given to the left of each emission spectrum. Note that the spacing between successive spectra is 0.25 eV. The width of the incident radiation was $\Delta h\nu = 60$ meV. This emission is consistent with final states corresponding to a $\pi \rightarrow \sigma^*$ promotion near *M*. (b) Simulated spectra in the same excitation region. (c) Core-hole crystal-momentum distributions for energies considered in (b).

intensities of two emission features at $h\nu'$ near 273 and 276 eV changing rapidly as a function of $h\nu$.

The crystal-momentum selectivity is particularly apparent as $h\nu$ is varied from 285 to 286.5 eV. This is illustrated in Fig. 7(a), which shows how the emission spectra change as the excitation energy is finely stepped through the π^* absorption threshold. Also, these spectra have been obtained using $\Delta h\nu \sim 60$ meV, compared with $\Delta h\nu \sim 150$ meV in Fig. 3, thereby increasing the momentum selectivity in the scattering. In Fig. 7(b), we illustrate the relevant portion of the π^* bands, i.e., along the *K*-*M* line. *M* is a saddle point in the π and π^* bands, so emission by π electrons is more sharp when $h\nu$ resonantly excites electrons there ($h\nu = 286$ eV). Meanwhile, there are two prominent features because of emission by σ electrons, at *K* ($h\nu' = 273$ eV) and *M* ($h\nu' = 276$ eV). Between *K* and *M*, the relevant σ band exhibits a cosinelike dispersion, whereas the π^* band is remarkably flat near *M*. Hence, as $h\nu$ approaches 286 eV from below, a cosecantlike emission feature, located around $h\nu' = 276$ eV, increases in strength dramatically. Direct and inverse photo-

emission, respectively, furnish insight into dispersion of occupied and unoccupied bands, and photoabsorption and x-ray emission provide insight into joint or total densities of states of unoccupied or occupied bands. The present fluorescence technique simultaneously probes the energies and dispersion characteristics of several occupied and unoccupied bands.

This ''*K*-to-*M* crossover'' has also been found in full-potential calculations, which omit core-hole effects[30] but not in a recent tight-binding calculation by van Veenendaal and Carra,[20] unless core-hole effects were included. Here, we find that it occurs in the same fashion regardless of core-hole effects. Data interpretation is complicated by the presence of ordinary fluorescencelike features, which are superposed on the rest of the emission, and exhibit a peak at the same energy as the sigma band at *M*. (Conversely, van Veenendaal and Carra's M σ emission would perhaps appear elsewhere than at their peak around 276 eV, based on an inspection of their band structure.) However, our present theory results show the peak clearly, even with no phenomenological inclusion of ordinary fluorescencelike features. Confusion can also arise with respect to the position of this peak, because of self-energy band-widening effects. In Fig. 8 is shown the core-hole crystal-momentum distribution in the simulated intermediate states as a function of $h\nu$. As expected, this is concentrated near *K* around threshold, and it spreads towards *M* at higher energy.

Figure 9(a) shows RIXS spectra obtained for excitation energies near 291.5 eV, which corresponds to the σ^* threshold in graphite. Analogous simulated spectra are presented in Fig. 9(b), and corresponding core-hole crystal-momentum distributions are shown in Fig. 9(c). An experimental emission feature is observed at $h\nu' \sim 281$ eV when $h\nu$ is tuned over a very narrow range centered on this threshold. This emission is consistent with final states corresponding to a $\pi \rightarrow \sigma^*$ promotion near *M*. (We have noted in Sec. II B that a more detailed representation of Zhu and Louie's quasiparticle band structure would place the σ^* resonance closer to 291.5 eV.) Absence of this emission feature when core-hole effects are omitted suggests this scenario: the cross section for scattering through intermediate states with σ^* electrons is enhanced compared to that for states with π^* electrons, because of core-hole effects, a hypothesis that is supported by Figs. 5(a) and 9(c). It is encouraging that the noted emission feature [indicated by an arrow in Fig. 9(b)] is enhanced in the calculations when core-hole effects are included.

A deeper problem involves the nature of emission because of C 1s-π electron-hole recombination. By symmetry considerations, this would be a weakly allowed process, because the core-hole amplitude in the relevant superpositions of intermediate states will vary like a π^* amplitude from site to site. Upon intermediate-state summation over sites, there will be strong destructive interference for emission by C 1s-π recombination. Experimentally, there is strong ''π emission,'' which decreases with detuning of $h\nu$ above the K edge. This is contrary to expectations, not only because of the copious emission observed, but also because density-of-states arguments would suggest an increase in the emission with increasing $h\nu$ above 284.5 eV. We have suppressed interference between intermediate-state channels with core holes on different sites within a unit cell. This invokes artificially what we interpret as an experimentally manifested symmetry breaking. If the symmetry breaking takes time to develop, it is natural that it would develop the most fully close to $h\nu = 284.5$ eV. Note also that all signatures of such symmetry breaking are conspicuously absent far below $h\nu = 284.5$ eV. If the symmetry breaking is ''accidental,'' such as its being a result of doping effects, we cannot address such a possibility quantitatively. For the present, we leave the intensity variation of this π emission as an unexplained feature in our paper. Such emission is found in the cited full-potential simulation of RIXS, which omits core-hole effects, but we have not found it in either the present pseudopotential calculation or in our past tight-binding study. We also emphasize that our inclusion of core-hole effects does not remedy this difficulty, nor do effects of finite photon momentum. Figure 10 presents RIXS spectra that do not suppress such interference. While some of the σ emission features are affected only slightly, the strengths of those at the lowest energies are affected substantially.

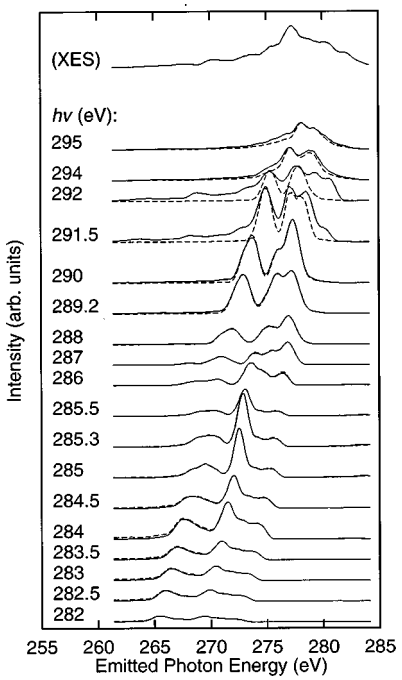

FIG. 10. Simulated RIXS spectra for graphite, which do not suppress the interference effect, mentioned in the text. Note the clear lack of emission from the π bands both above and below the core threshold.

XAS results for hBN are presented in Fig. 11, and reveal the strong π^* exciton (1.5 eV bound, theoretically) and characteristic ''camel's-back'' σ^* excitonic resonance feature. RIXS results are also presented in Fig. 11, and the band structure is shown in Fig. 12. As for HOPG, solid curves denote calculated spectra with core-hole effects included, and dashed curves denote calculated spectra omitting core-hole effects. Spectral features are similar for all $h\nu$ considered. The 11 and 16 eV Stokes-shifted emission features are attributed to final states with a π^* electron and a σ hole near *L* or *M*. As in HOPG, analysis of the core-hole momentum distribution in the intermediate state was carried out, and we have found that it is concentrated near *M* for $h\nu = 192$ eV, i.e., where the π^* conduction-band minimum is found. We

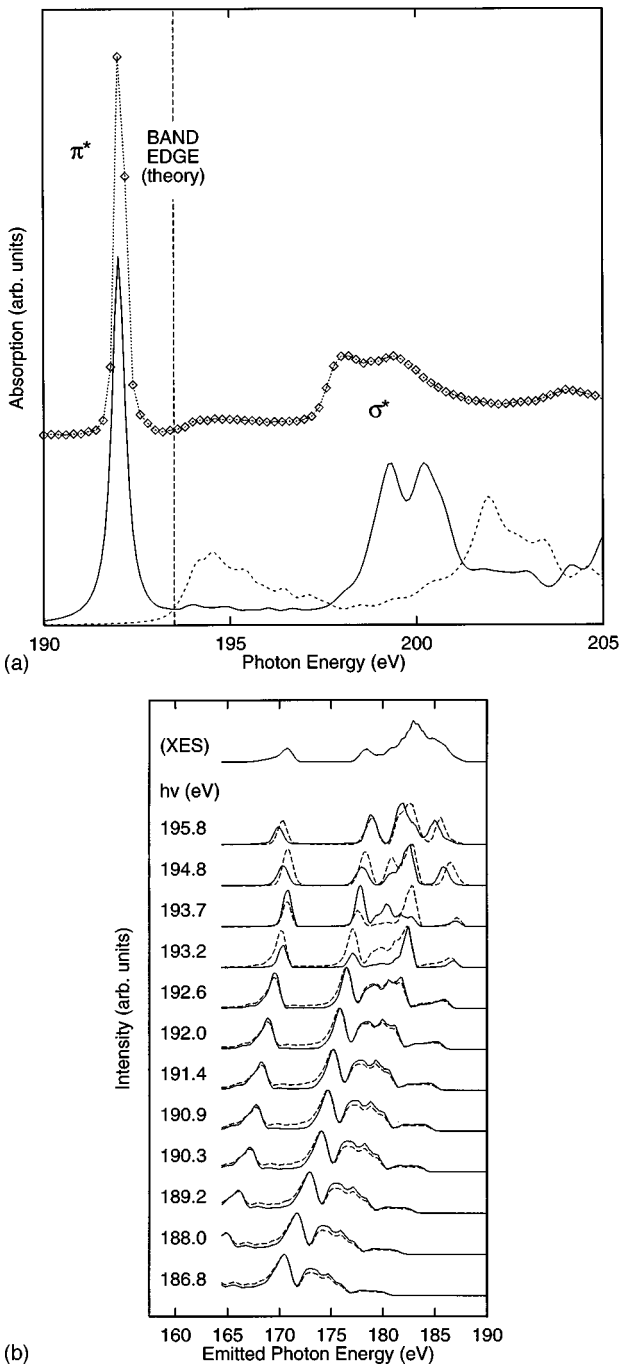

FIG. 11. Simulated x-ray absorption spectrum [Fig. 11(a)] and RIXS [Fig. 11(b)] for hBN. Solid lines correspond to calculations made with core-hole effects included, whereas dashed lines give the results of calculations based on a noninteracting (one-electron) picture.

have not found a theoretical analog to the observed feature ''*C*,'' and we attribute the relative weakness of the 11 eV feature compared to experiment to neglect of final-state valence-hole effects. Such effects would cause final states with the electron and valence hole in close proximity to be enhanced at lower final-state energies, i.e., higher emitted photon energies in RIXS.

The largest departure between experiment and simulation for hBN occurs at $h\nu = 193.7$ eV. Experimentally there is an abrupt change in the character of the emission from the

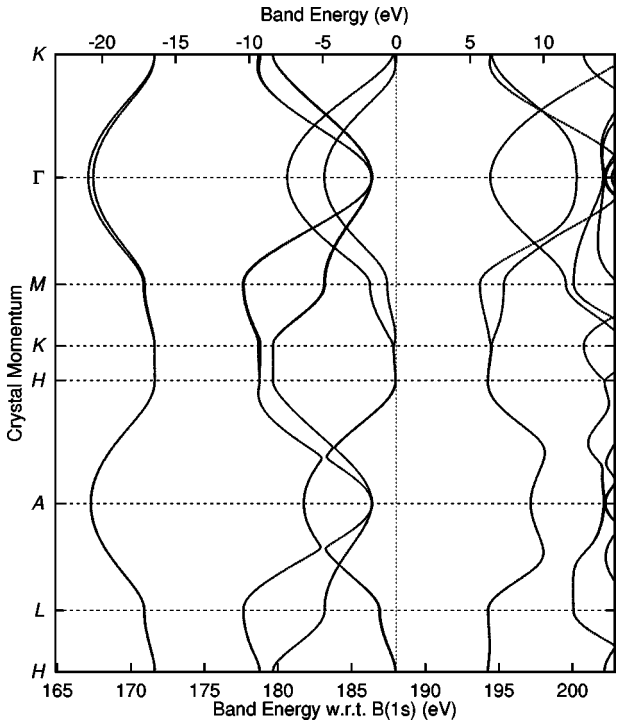

FIG. 12. Band structure of hexagonal boron nitride.

Raman-like mode (with the p-JDOS tracking the excitation energy) to an emission spectrum equivalent to the normal or nonresonant *B* 1s fluorescence. This failure of the simulation suggests that effects neglected in the theory (valence excitons, phonons, etc.) can contribute significantly to the observed RIXS. It is interesting that the inclusion of core-hole effects does not resolve this departure, because it is well known that hBN has a very strong core-hole exciton.

V. SUMMARY

To summarize, we have demonstrated that the resonant inelastic x-ray scattering present in resonant fluorescence spectra obtained below and above a core-level absorption threshold may be utilized to probe the band structure of a material. To a large degree, the scattering regimes below and above threshold are described by the same scattering physics of coherent fluorescence as first put forward by Ma,[4] based on the quasiparticle band structure of graphite and hBN. This remains true, even though describing XAS and RIXS *total* fluorescence yields involves accounting for core-hole effects. We find that fluorescence spectra can be almost uniformly enhanced or suppressed, depending on the excitation energy, when core-hole effects are considered. This follows from the notion that the electron-core-hole attraction mostly enhances the superposition of intermediate states achieved without influencing it much otherwise. However, we have established that this notion fails to varying degrees when one considers excitation into several different types of intermediate states, e.g., both π^* and σ^* core-hole excitonic resonances.

The intrinsic strengths of soft-x-ray fluorescence for probing the bulk-sensitive and element-specific and/or momentum-resolved electronic structure of materials demonstrates the potentially broad utility of the technique.[28,31,32] The results presented here and elsewhere are clearly indica-

tive of its potential for probing the electronic structure of more complex systems, particularly buried thin films and heterointerfaces, which are less accessible to other techniques.

ACKNOWLEDGMENTS

This paper was supported at VCU by a Research Corporation Cottrell College Science Award No. CC4526, a Jeffress Trust Memorial Foundation Grant No. J-424, and by a Faculty Grant-in-Aid at Virginia Commonwealth University. The paper was also supported by the Division of Materials Science, Office of Basic Energy Sciences, and performed under the auspices of the U.S. Department of Energy by Lawrence Livermore National Laboratory under Contract No. W-7405-ENG-48, by National Science Foundation Grants Nos. DMR-9017996 and DMR-9017997, by a Science Alliance Center for Excellence Grant from the University of Tennessee, by the U.S. Department of Energy (DOE) Contract No. DE-AC05-84OR21400 with Oak Ridge National Laboratory, and by the Louisiana Educational Quality Support Fund and DOE-EPSCOR Grant No. LEQSF (93-95)-03 at Tulane University. This experiment was performed at the Advanced Light Source, which is also supported by the Office of Basic Energy Sciences, U.S. Department of Energy, under Contract No. DE-AC03-76SF00098.

*Author to whom correspondence should be addressed. Electronic address: jacarlis@vcu.edu

[1] H. Renevier, J. L. Hodeau, P. Wolfers, and S. Andrieu, Phys. Rev. Lett. **78**, 2775 (1997); E. D. Specht and F. J. Walker, Phys. Rev. B **47**, 13 743 (1993); F. J. Walker, E. D. Specht, and R. A. McKee, Phys. Rev. Lett. **67**, 2818 (1991).

[2] A. Barbara, J. M. Tonnerre, M. C. SaintLager, and F. Bartolome, J. Magn. Magn. Mater. **165**, 87 (1998).

[3] See, for instance, T. Iwazumi, K. Kobayashi, S. Kishimoto, and T. Nakamura, Phys. Rev. B **56**, 14 267 (1997).

[4] Y. Ma, Phys. Rev. B **49**, 5799 (1994); P. D. Johnson and Y. Ma, *ibid.* **49**, 5024 (1994); P. Carra, M. Fabrizio, and B. T. Thole, Phys. Rev. Lett. **74**, 3700 (1995).

[5] E. L. Shirley, Phys. Rev. Lett. **80**, 794 (1998).

[6] J. A. Carlisle, E. L. Shirley, L. J. Terminello, E. A. Hudson, J. J. Jia, T. A. Callcott, D. L. Ederer, R. C. C. Perera, and F. J. Himpsel, Phys. Rev. Lett. **74**, 1234 (1995).

[7] Y. Ma, N. Wassdahl, P. Skytt, J. Guo, J. Nordgren, P. D. Johnson, J.-E. Rubensson, T. Boske, W. Eberhardt, and S. D. Keven, Phys. Rev. Lett. **69**, 2598 (1992).

[8] See, for instance, D. L. Ederer, T. A. Callcott, and R. C. C. Perera, Synchrotron Radiation News **7**, 29 (1994).

[9] E. J. Nordgren, J. Phys. IV **7**, 9 (1997).

[10] L. Yi, H. Agren, F. Gel'mukhanov, G. Jinghua, and J. Nordgren, Phys. Rev. B **52**, 14 479 (1996); J.-H. Guo, P. Glans, P. Skytt, N. Wassdahl, and J. Nordgren, *ibid.* **52**, 10 681 (1995); G. Jinghua, P. Skytt, N. Wassdahl, and J. Nordgren, Chem. Phys. Lett. **235**, 152 (1995).

[11] A. Nilsson, M. Weinelt, T. Wiell, and P. Bennich, Phys. Rev. Lett. **78**, 2847 (1997).

[12] T. Wiell, H. Tillborg, A. Nilsson, and N. Wassdahl, Surf. Sci. **304**, L451 (1994).

[13] P. Glans, K. Gunnelin, P. Skytt, J.-H. Guo, and J. Nordgren, Phys. Rev. Lett. **76**, 2448 (1996).

[14] J.-E. Rubensson, D. Muller, R. Shuker, D. L. Ederer, C. H. Zhang, J. Jia, and T. A. Callcott, Phys. Rev. Lett. **64**, 1047 (1990).

[15] J. Luning, J.-E. Rubensson, C. Ellmers, and S. Eisebitt, Phys. Rev. B **56**, 13 147 (1997).

[16] J. J. Jia, T. A. Callcott, E. L. Shirley, J. A. Carlisle, L. J. Terminello, A. Asfaw, D. L. Ederer, F. J. Himpsel, and R. C. C. Perera, Phys. Rev. Lett. **76**, 4054 (1996); W. L. O'Brien, J. Jia, Q.-Y. Dong, T. A. Callcott, K. E. Miyano, D. L. Ederer, D. R. Mueller, and C.-C. Kao, *ibid.* **70**, 238 (1993).

[17] A. Agui, S. Shin, M. Fujisawa, and Y. Tezuka, Phys. Rev. B **55**, 2073 (1997).

[18] C. B. Stagarescu, L. C. Duda, K. E. Smith, and J. H. Guo, Phys. Rev. B **54**, 17 335 (1996).

[19] P. A. Brühwiler, P. Kuiper, O. Eriksson, R. Ahuja, and S. Svensson, Phys. Rev. Lett. **76**, 1761 (1996); J. A. Carlisle, E. L. Shirley, L. J. Terminello, E. A. Hudson, J. J. Jia, T. A. Callcott, D. L. Ederer, and F. J. Himpsel, *ibid.* **76**, 1762 (1996).

[20] M. van Veenendaal and P. Carra, Phys. Rev. Lett. **78**, 2839 (1997).

[21] For more information, see http://www-als.lbl.gov/

[22] J. J. Jia, T. A. Callcott, J. Yurkas, A. W. Ellis, F. J. Himpsel, M. G. Samant, J. Stohr, D. L. Ederer, J. A. Carlisle, E. A. Hudson, L. J. Terminello, R. C. C. Perera, and D. K. Shuh, Rev. Sci. Instrum. **66**, 1394 (1995).

[23] P. A. Brühwiler, A. J. Maxwell, C. Puglia, A. Nilsson, S. Anderson, and N. Mårtersson, Phys. Rev. Lett. **74**, 614 (1995); A. Chaiken, L. J. Terminello, J. Wong, and G. L. Doll, Appl. Phys. Lett. **63**, 2112 (1993).

[24] E. L. Shirley, Phys. Rev. B **54**, 16 464 (1996).

[25] X. Zhu and S. G. Louie, in *Topics in Computational Materials Science*, edited by C. Y. Fong (World Scientific, Singapore, 1997), 96.

[26] X. Blase, A. Rubio, S. G. Louie, and M. L. Cohen, Phys. Rev. B **51**, 6868 (1995).

[27] Z. H. Levine and S. G. Louie, Phys. Rev. B **25**, 6310 (1982); M. S. Hybertsen and S. G. Louie, *ibid.* **37**, 2733 (1988).

[28] J. A. Carlisle, L. J. Terminello, E. A. Hudson, J. J. Jia, T. A. Callcott, D. L. Ederer, R. C. C. Perera, and F. J. Himpsel, Appl. Phys. Lett. **67**, 34 (1995).

[29] P. E. Batson, Phys. Rev. B **48**, 2608 (1993).

[30] B. N. Harmon and J. Y. Rhee (private communication).

[31] J. A. Carlisle, A. Chaiken, R. P. Michel, L. J. Terminello, T. A. Callcott, J. J. Jia, and D. L. Ederer, Phys. Rev. B **53**, R8824 (1996).

[32] L.-C. Duda, C. B. Stagarescu, J. Downes, K. E. Smith, D. Doppalapudi, T. D. Moustakas, J. Guo, and J. Nordgren, Phys. Rev. B **58**, 1928 (1998).